

IMPULSE RADIATING ANTENNAS, PART III

Everett G. Farr¹ and Carl E. Baum²

¹Farr Research, Inc.
Albuquerque, NM 87123

²Phillips Laboratory,
Kirtland AFB, NM 87117

ABSTRACT

In this paper we continue our general discussion of Impulse Radiating Antennas (IRAs), which has been carried on during the first two Ultra-Wideband, Short-Pulse Electromagnetics conferences. IRAs are a class of antennas that consist of a TEM feed section and either a lens or reflector to focus the aperture field. We summarize here much of the more recent information, including new antenna designs, new calculation methods, and an optimization of the impedance of the lens IRA.

First, we explore a wide variety of new IRA designs that include two reflecting or refracting surfaces. By using two surfaces, one can achieve considerable additional flexibility in design. This flexibility allows very compact designs, and also allows additional choices of feed impedance.

Next, we consider the optimal feed impedance for long TEM horns and lens IRAs. We consider both TEM horns whose plates are flat, and whose plates are confined to a circular arc. We also consider both infinite apertures and circular apertures of finite radius. The optimal impedance is determined as the impedance that provides the highest radiated field for a given input power.

Finally, we calculate the field radiated from a four-wire aperture, both on- and off-boresight. This is an approximation to the aperture field of a four-armed reflector IRA.

I. INTRODUCTION

The theory of Impulse Radiating Antennas has been building for some time [1,2]. Simple models are now available for the radiated field for both lens and reflector designs. Sketches of lens and reflector IRAs are shown in Figure 1.1.

In this paper we extend the theory in several key areas. First, we consider a broad range of new designs which make use of two reflecting or refracting surfaces. Second, we calculate the optimal impedance for infinitely long TEM horns and lens IRAs. Finally, we calculate the radiated field from a four-wire aperture on- and off-boresight.

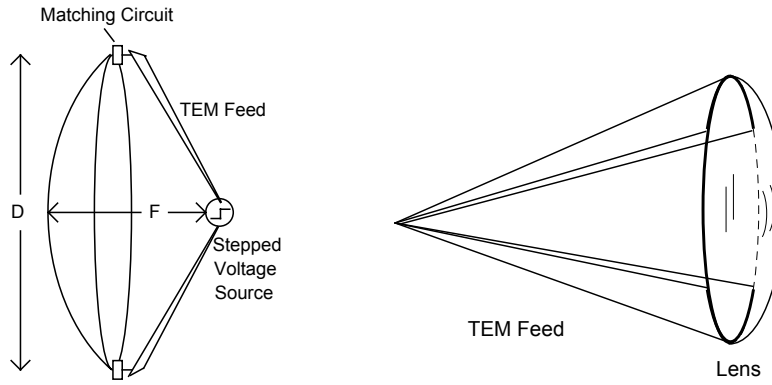


Figure 1.1. A reflector IRA (left) and a lens IRA (right).

II. IRAS WITH TWO REFLECTING OR REFRACTING SURFACES

Several new antenna designs can be fabricated with a combination of two reflecting and/or refracting surfaces[3]. A ReLIRA is an IRA consisting of both a reflector and a lens, and an example is shown in Figure 2.1. It consists of a TEM feed and a planar reflector, all embedded in a dielectric medium, with a prolate spheroidal lens[4] to focus the rays. Note that a prolate spheroid is just an ellipse that has been rotated around its major axis.

The lens for this antenna forces all the high-frequency rays to arrive at some aperture plane concurrently, as shown in Figure 2.2. To satisfy the condition, the lens shape is described by

$$\sqrt{\epsilon_1} = \sqrt{\epsilon_1} r + \sqrt{\epsilon_2} (-z) \quad (2.1)$$

where all the symbols are shown in Figure 2.2. This results in a ellipse of revolution that is described by

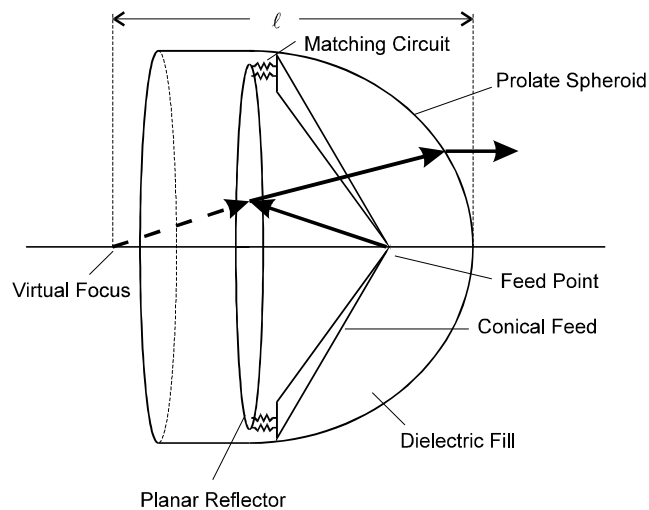


Figure 2.1. ReLIRA with Planar Reflector and Prolate Spheroidal Lens, two-arm version.

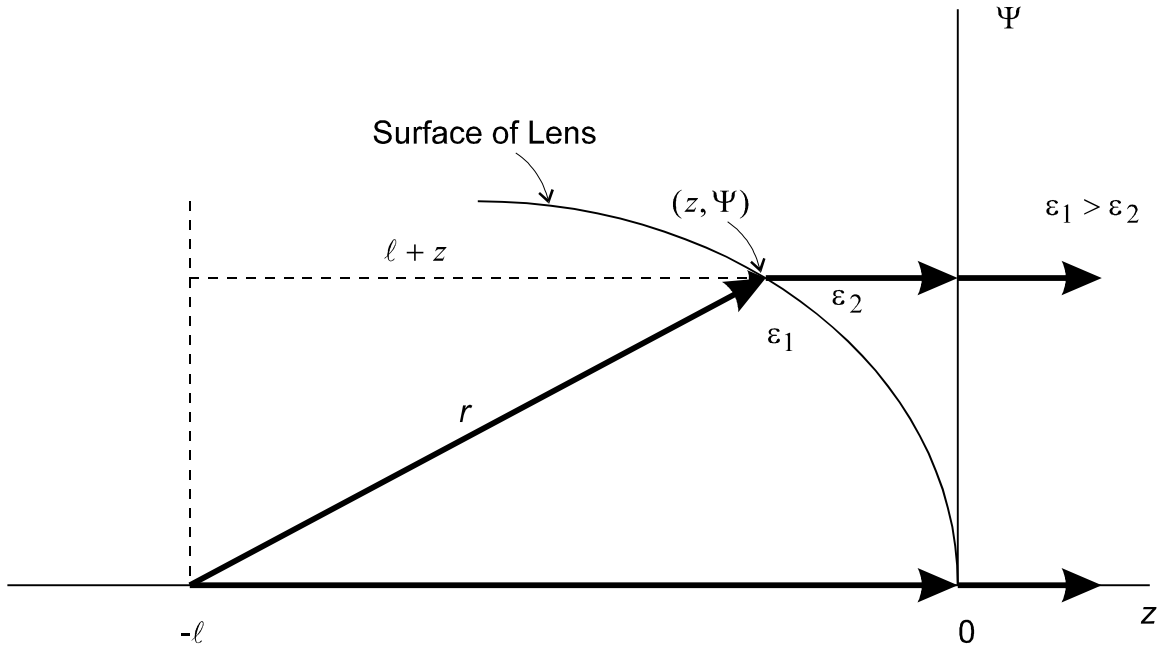


Figure 2.2. Geometry of the prolate spheroid dielectric interface (an ellipse when projected into the Ψ - z plane).

$$\frac{(z+a)^2}{a^2} + \frac{\Psi^2}{b^2} = 1, \quad a = \frac{\ell}{1+q}, \quad b = \sqrt{\frac{1-q}{1+q}}, \quad q = \sqrt{\epsilon_2 / \epsilon_1} \quad (2.2)$$

where a and b are the major and minor axes of the ellipse. Details of the derivation are provided in [3].

There are a number of variations of this antenna, the first of which is the Solid Dielectric Lens IRA. This combines a TEM horn embedded in a dielectric, with a prolate spheroidal lens interface. A sketch of this configuration is shown in Figure 2.3. Note that the feed point of the TEM horn is located at a focus of the prolate spheroid. Other variations might include using either a hyperboloidal reflector (with a prolate spheroidal lens) or a paraboloidal reflector (with a planar lens). These two configurations are shown in Figure 2.4. While the version with a paraboloidal reflector may seem to be a trivial case, it may have some use in applications requiring high mechanical stability (shock-hardened) or in applications requiring a lower feed impedance.

Yet another variation is the Split IRA (SPIRA), an example of which is shown in Figure 2.5. This is a technique for placing two half IRAs in close proximity, in order to implement separate transmit and receive antennas in a compact design. In this design, each of the two half IRAs share a thick ground plane, through which feed cables are run. Any of the designs previously discussed in this paper, or any of the classical reflector or lens IRA designs could be implemented in such a fashion. An example of such a design, using an ReLIRA with a planar reflector and prolate spheroidal lens is shown in Figure 2.5.

An interesting feature of the Split IRA is that one can achieve a very low feed impedance. By using two arms for each half, the feed impedance is typically 100Ω in air. If the dielectric material has a relative dielectric constant of four, then the input impedance is 50Ω . This is a convenient impedance for matching to a source. In addition, this is a single-ended impedance, so it matches well to a coaxial cable input.

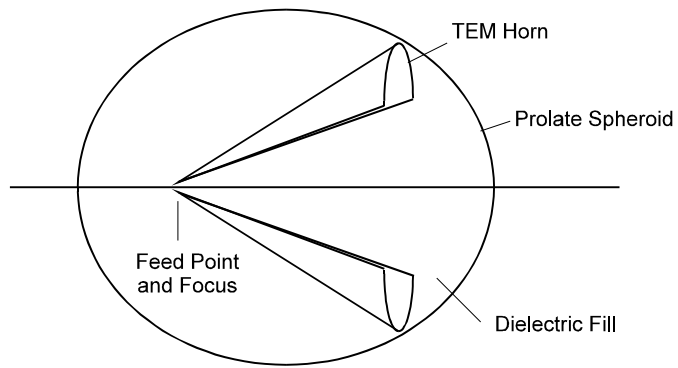


Figure 2.3. A solid dielectric lens IRA.

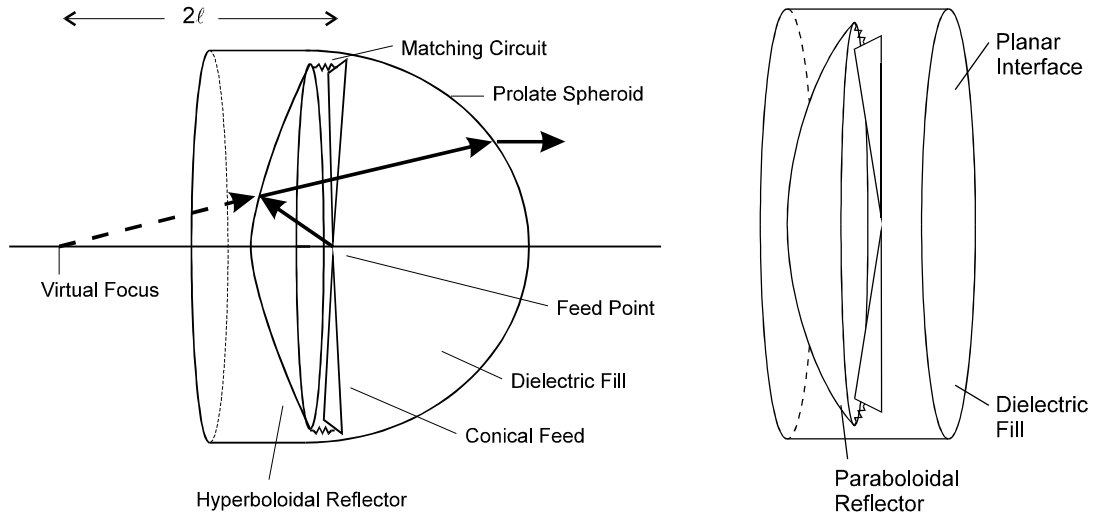


Figure 2.4. ReLIRAs with a hyperboloidal reflector and prolate spheroidal lens (left) and with a paraboloidal reflector and planar lens (right). (Two-arm versions are shown.)

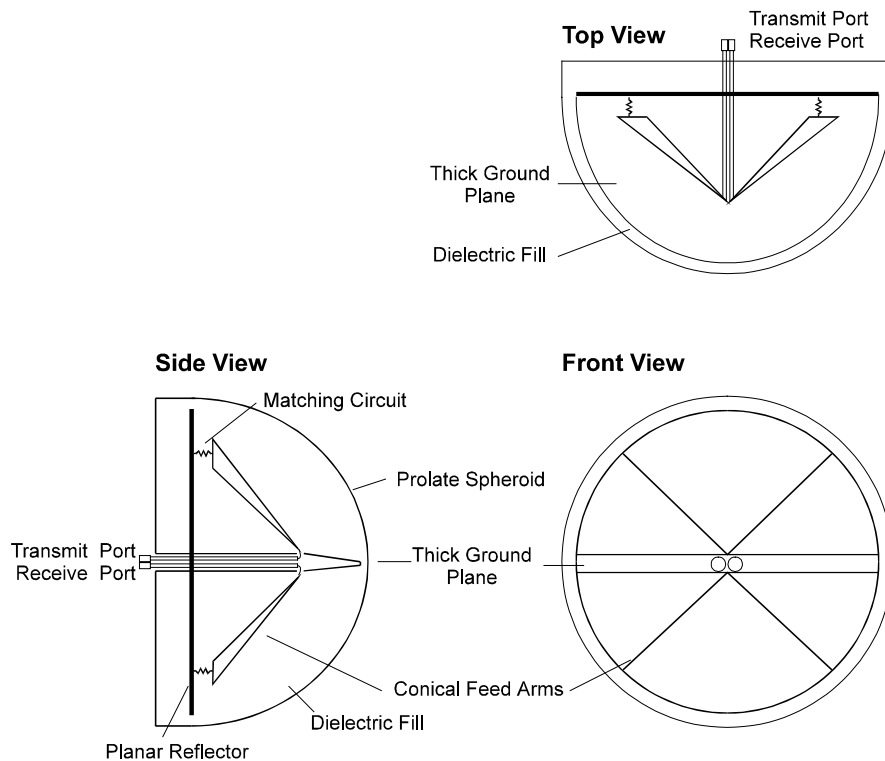


Figure 2.5. An example of a SPIRA, using a flat plate reflector and a prolate spheroidal lens. (Four-arm version is shown.)

III. IMPEDANCE OPTIMIZATION OF LONG TEM HORN AND LENS IRA

In previous papers[2,5], we demonstrated a method for optimizing the impedance of two-wire and four-wire apertures. These apertures corresponded to the aperture fields for two-arm and four-arm reflector IRAs. Let us now optimize the impedance of long TEM horns, or lens IRAs. This material originally appeared in [6].

We wish to optimize the impedance of the flat plates of a TEM horn, under the constraint that they lie within a circle of radius a_o , as shown in Figure 3.1. Thus, we search for the aspect ratio, b/a , which optimizes the radiated field for constant input power. We treat two cases here, one with the flat plates located in free space, and the other with a conducting plate that blocks fields outside the circle. We optimize the impedance in an early-time sense, using the static fields in the aperture.

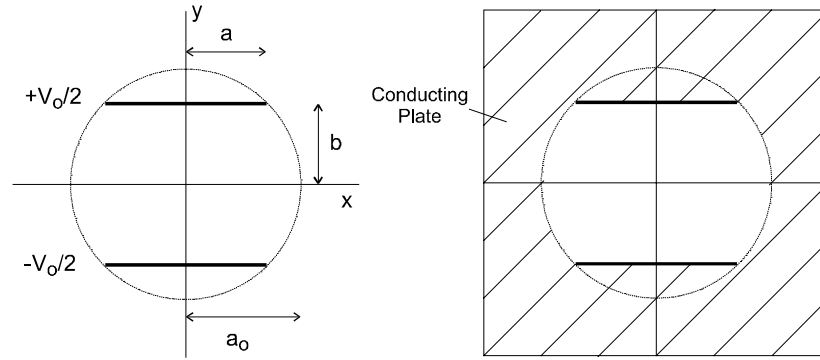


Figure 3.1. Two cases for optimizing the radiated field of a flat TEM horn, infinite aperture (left) and blocked aperture (right).

To optimize the impedance, we must find the quasi-static electric field in the aperture between two plates. First, we calculate the characteristic impedance of the feed. The impedance is determined from [7,8]

$$f_g = \frac{K(m_1)}{K(m)} , \quad m_1 = 1 - m , \quad \sin(\phi_o) = \sqrt{\frac{1}{m} \left(1 - \frac{E(m)}{K(m)} \right)} \quad (3.1)$$

$$\frac{a}{b} = \frac{2}{\pi} [K(m)E(\phi_o|m) - E(m)F(\phi_o|m)]$$

where $K(m)$ and $E(m)$ are the complete elliptic integrals of the first and second kind, and $F(\phi_o|m)$ and $E(\phi_o|m)$ are the incomplete elliptic integrals of the first and second kind. Furthermore, $f_g = Z_c/Z_o$, where $Z_o = 376.727 \Omega$. To find f_g for a given value of b/a , one must solve numerically the above set of equations. At low impedances, an asymptotic form is used for the impedance [8],

$$f_g = \frac{b/a}{1 + \frac{b/a}{\pi} \left[1 + \ln \left(\frac{2\pi}{b/a} \right) \right]} \quad (3.2)$$

This form was used for $b/a < 0.3$. Since the aperture is constrained to be of radius a_o , the relationship between a and b is expressed as

$$\frac{a^2}{a_o^2} + \frac{b^2}{a_o^2} = 1 \quad , \quad b = \frac{a_o}{\sqrt{1 + (a/b)^2}} \quad , \quad a = \frac{a_o}{\sqrt{1 + (b/a)^2}} \quad (3.3)$$

To obtain the radiated fields, we find the static fields in the aperture. Thus, we need to find a potential function in the form

$$\begin{aligned} \zeta &= x + jy \\ w(\zeta) &= u(\zeta) + jv(\zeta) \quad , \quad x, y, u, \text{ and } v \text{ are all real} \end{aligned} \quad (3.4)$$

When cast into this form, the aperture field and feed impedance are [7,8]

$$E_y(x,y) = -\frac{V_o}{\Delta u} \frac{\partial u(x,y)}{\partial y} \quad , \quad f_g = \frac{\Delta u}{\Delta v} \quad (3.5)$$

where Δu is the change in u from one conductor to the other, and Δv is the change in v as one goes around one conductor. We now need a suitable complex mapping to fit the problem.

The potential function that describes the aperture is [7, eqn. 2.15]

$$\frac{\zeta}{b} = \frac{2j}{\pi} [K(m) E(w|m_1) + w \times (E(m) - K(m))] \quad (3.6)$$

This is the simplest form. Another form is used in [8,9], but it is less convenient because the conductors are located on surfaces of constant v instead of the more customary constant u . As a cautionary note, we point out that most numerical packages expect the first argument of the incomplete elliptic function, $E(w|m)$, to be in the form of an angle. Thus, the incomplete elliptic integral has to be cast into the form of $E(\text{am}(w|m)|m)$, where $\text{am}(w|m) = \arcsin(\text{sn}(w|m))$ is the Jacobian amplitude function. A plot of the resulting complex mapping appears in Figure 3.2.

The figure of merit we use for the radiated field is the transient power gain normalized to constant input power, as defined in [2,5,6,10]. Thus, we have

$$G_p = \frac{h_a}{\sqrt{f_g}} \quad (3.7)$$

where h_a is the normalized integral over the aperture field [11],

$$h_a = -\frac{f_g}{V_o} \iint_{S_a} E_y(x', y') dx' dy' \quad (3.8)$$

and S_a is the total surface over which radiation occurs. This integral will be calculated for the two configurations as a function of Z_c .

Let us pause for a moment, to consider whether the figure of merit, G_p , makes sense. To see why our expression of gain in (3.7) is reasonable, we recall that the fast part of the field radiated from an aperture on boresight is [2,5,6]

$$\begin{aligned} E_{rad}(t) &= -\frac{h_a}{2\pi r c f_g} \frac{dV(t)}{dt} \\ E_{rad}(t) &= -\frac{G_p}{2\pi r c} \frac{d(V(t)/\sqrt{f_g})}{dt} \end{aligned} \quad (3.9)$$

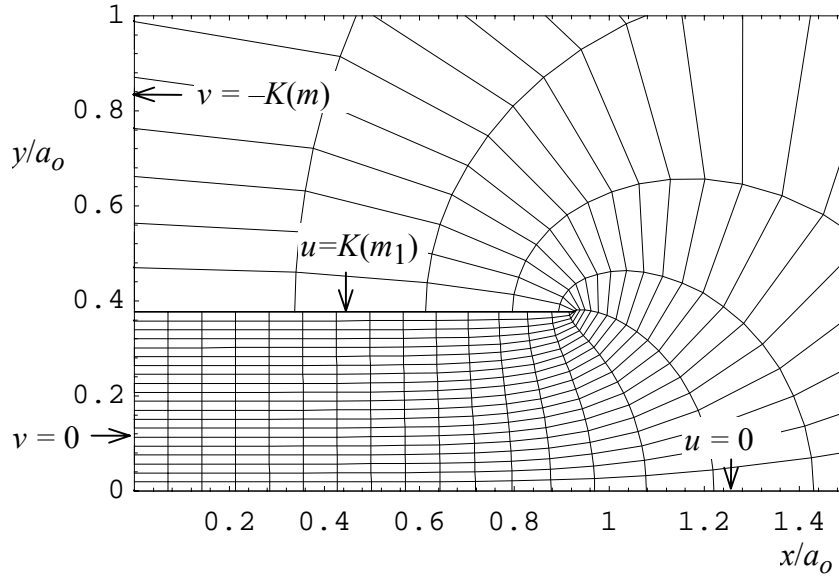


Figure 3.2. Complex potential map of the parallel plate configuration, for $Z_c = 100 \Omega$.

Furthermore, the received voltage for an incident field on boresight is

$$\begin{aligned} V_{rec}(t) &= -h_a E_{inc}(t) \\ \frac{V_{rec}(t)}{\sqrt{f_g}} &= -G_p E_{inc}(t) \end{aligned} \quad (3.10)$$

Thus, both the radiated field and the received voltage are proportional to power gain. Note also that all the voltages are cast into the form of square root of power, by dividing by $\sqrt{f_g}$. On this basis, our definition of the figure of merit seems reasonable.

A. Flat Plates with Infinite Aperture

We now calculate h_a and G_p for two cases. First, we consider the case of an infinite aperture, as shown on the left in Figure 3.1. In this case, it is particularly simple to calculate h_a , since it can alternatively be expressed in terms of the dipole moment of the charge in the aperture [11]. Thus,

$$h_a = \frac{1}{2} \frac{\iint q(x,y) y dA}{\iint q(x,y) dA} \quad (3.11)$$

where $q(x,y)$ is the charge density on the conductors, and the integrals are carried out over all the conductors in the aperture. Since all the charge is located at $y = \pm b$, the value of h_a is calculated trivially as

$$h_a = b \quad (3.12)$$

We have plotted h_a/a_0 as a function of Z_c in Figure 3.3, on the left. As expected, at high impedances it approaches unity asymptotically. This is the expected result because for a pair of thin wires, we know from [11] that $h_a = a_0$. Finally, we have plotted the power gain, $G_p = h_a / \sqrt{f_g}$, in Figure 3.3, on the right. The peak occurs at $Z_c = 242.3 \Omega$, where the power gain is $1.09 \times a_0$. At this point, $b/a = 1.82$.

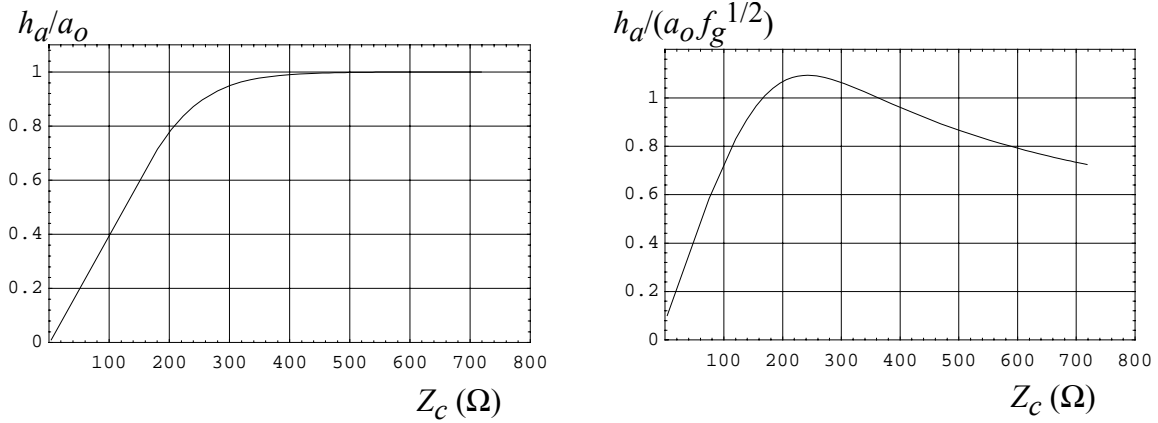


Figure 3.3. Normalized aperture height for the infinite aperture with flat plates (left) and the corresponding figure of merit (right).

B. Flat Plates with Blocked Aperture

Next, we calculate h_a for the case of a blocked aperture, as shown on the right in Figure 3.1. This is the normal case of interest to the antenna designer. Only a portion of the aperture field is included in the aperture integral, because only that portion is focused.

To calculate h_a , we express it as a contour integral [2,5,11], i.e.,

$$h_a = -\frac{4}{\Delta v} \oint_{C_a} v(\zeta) dy \quad (3.13)$$

where Δv is the change in v around a conductor. Furthermore, C_a is a contour consisting of four segments which surround one quadrant of the exposed portion of the aperture, as shown in Figure 3.4. To calculate this integral, we note that the integrals over C_1 and C_3 are identically 0, since there is no change in y . Furthermore, the integral over C_4 is also zero, because $v = 0$ there. Therefore, we need only calculate the integral over C_2 .

Calculating the integral over C_2 presents us with a challenge, because there is no easy way to calculate $v(\zeta)$. Normally, one would find v from the complex contour mapping, i.e., equation (3.6). But in the present case there is no simple way to invert the contour mapping to find v in terms of ζ . Thus, one would have to solve (3.6) numerically for $v(\zeta)$ at each location on the arc. Since we must also calculate the integral along this path, this becomes computationally expensive.

A simpler method is to just assume that the contour C_2 is along a contour of constant v , instead of being along a portion of a circular arc. This is rigorously true in the limit of high impedances, $b/a \rightarrow \infty$, because the conductors become thin wires at that point. Since we know the optimal values will occur at relatively high values of b/a , the approximation is reasonable. Thus, we search numerically for the value of v that intersects the circle at $(x, y) = (a_o, 0)$, and use that for our contour of constant v_o . From (3.6), we solve numerically the following for v_o ,

$$\frac{a_o}{b} = \frac{2j}{\pi} [K(m) E(jv_o|m_1) + jv_o \times (E(m) - K(m))] \quad (3.14)$$

After finding v_o , and using the fact that $\Delta v = 2K(m)$, we find the aperture height to be

$$h_a = -\frac{2bv_o}{K(m)} \quad (3.15)$$

Note that v_o is a negative number, so h_a is positive, as it must be. We estimate the error in this procedure to be a few percent.

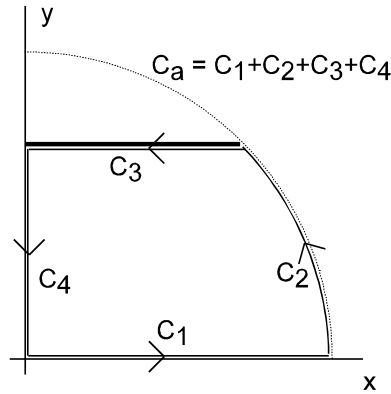


Figure 3.4. Definition of the contour C_a .

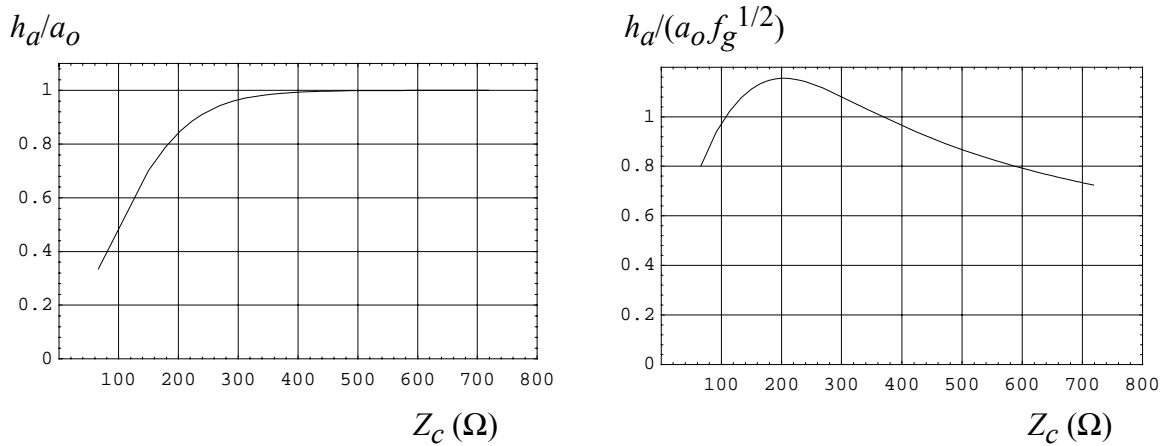


Figure 3.5. Normalized aperture height for the blocked aperture with flat plates (left), and the normalized figure of merit (right).

The results for h_a are plotted in Figure 3.5 (left), and the power gain is plotted on the right of the same figure. The peak gain occurs at $Z_c = 203.7 \Omega$, where the power gain is $1.16 \times a_o$. At this point, $b/a = 1.28$.

It is interesting to compare the results for the blocked aperture to those with the infinite aperture. One might expect that an infinitely large aperture would have better performance, but that is not the case. The blocked aperture actually has a slightly better power gain, with a value of $1.16 \times a_o$, compared to $1.09 \times a_o$ for the infinite aperture. The likely reason for this is that we have blocked out fields that have a negative contribution to the total radiated field, just above the top plate and just below the bottom plate. Therefore, if one wanted to improve the performance of a simple long TEM horn, one would block out the portion of the aperture fields just above and below the top and bottom plates.

A similar case with curved plates confined to a circular arc was treated in [6]. The optimal impedance for that case was $f_g = 0.5$, or $Z_c = 376.727 / 2 \Omega$, which occurs with plates with angular widths of 90° . This is true for both the blocked aperture and for the infinite aperture. It was demonstrated in [12] that these two cases are equivalent. At this impedance, we have $h_a = 0.85 \times a_o$, and $G_p = 1.20 \times a_o$, where a_o is the aperture radius.

IV. RADIATION FROM FOUR-WIRE APERTURES

Finally, we consider the radiated field pattern of a four-wire aperture. This is an approximation to the four-arm reflector Impulse Radiating Antenna. In previous papers [2,13] we considered the radiated field for a two-wire aperture, so the technique used here is essentially the same. The only change is that the aperture field is described by a different aperture potential [14]. Note that only the fast part of the radiated field is considered here.

When the conical geometry is projected onto a plane, we have an aperture field that is created from four conductors, as shown in Figure 4.1. The potential function is calculated by adding the potential for two two-wire problems, including translation. The potential function for a single pair of wires, where the charge centers are located at $(x=0, y/a = 1)$, is

$$w_2(\zeta) = 2j \operatorname{arccot}(\zeta/a) = \ln\left(\frac{\zeta - ja}{\zeta + ja}\right) \quad (4.1)$$

where a is the aperture radius. Here, $\zeta = x + jy$ is the location in the Cartesian coordinate space. This potential function is plotted in [13, Figure 2]. The complex potential for the four-wire case is just a sum of two two-wire potentials that have been shifted and rescaled,

$$w_4(\zeta) = w_2((\zeta/a + \sqrt{2})/\sqrt{2}) + w_2((\zeta/a - \sqrt{2})/\sqrt{2}) \quad (4.2)$$

This function is complex, i.e., has both real and imaginary parts. Let us therefore set

$$u(\zeta) = \operatorname{Re}(w_4(\zeta)) \quad , \quad v(\zeta) = \operatorname{Im}(w_4(\zeta)) \quad (4.3)$$

We can plot contours of constant u and v , and these are shown in Figure 4.2, for the upper right quadrant. The conductors correspond to a contour of constant u .

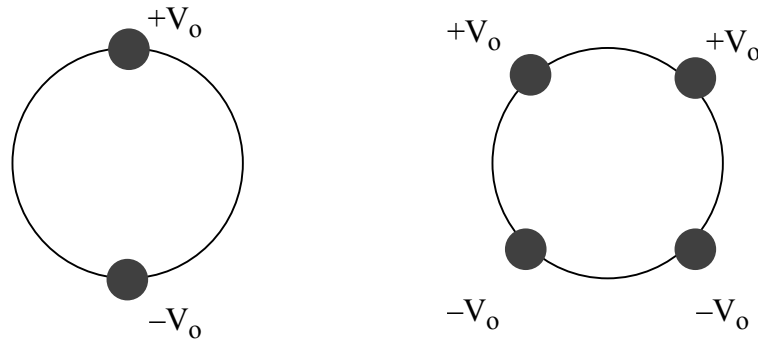


Figure 4.1. The apertures for a two-wire and four-wire configuration.

To calculate the radiated field, we need the aperture fields and the normalized aperture potentials. The aperture field is

$$E_y(x, y) = \frac{-(2V_0) \bar{\partial} u(x, y)}{\Delta u \quad \partial y} \quad (4.4)$$

where $2V_0$ is the voltage between the top and bottom conductors, and Δu is the change in u between the two conductors.

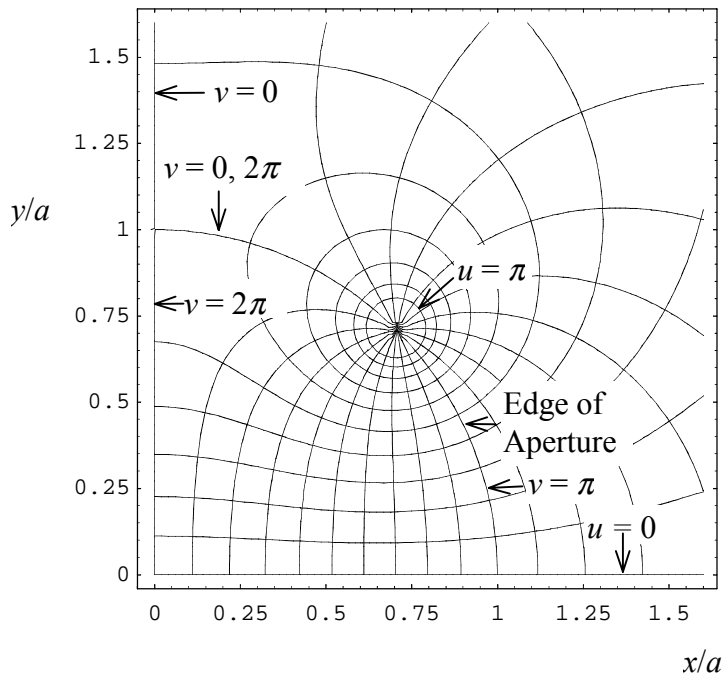


Figure 4.2. Contour map for $w_4(\zeta)$. Increments for u and v are $\pi/10$.

The normalized potentials are integrals over linear paths in the aperture field. We need to calculate these because the radiated field is proportional to them. The normalized potentials for the H-plane calculation is

$$\Phi^{(h)}(x) = -\frac{1}{(2V_o)} \int_{C_1(x)} E_y dy \quad (4.5)$$

where the contour $C_1(x)$ is a vertical line cut through the aperture plane, as shown in Figure 4.3. To simplify this H-plane integral, one substitutes (4.4) into (4.5), generating

$$\Phi^{(h)}(x) = \frac{1}{\Delta u} \int_{C_1(x)} \frac{\partial u}{\partial y} dy = \frac{2}{\Delta u} u\left(x, \sqrt{a^2 - x^2}\right) \quad (4.6)$$

We can now calculate $u(x,y)$ as the real part of the potential function given in (4.2). Note that the value of $u(x,y)$ is a maximum when it cuts through the conductors. At this point, the value of $u(x,y)$ is $u_o = \pi f_g$, where f_g is the relative impedance for a single pair of arms located on opposite sides of the circle (typically $f_g = 400 \Omega \epsilon / 377 \Omega$). Note also that for values of x that cut through the conductors, the normalized potential is unity. This normalized potential function is plotted in Figure 4.4 (left), for a few different values of f_g .

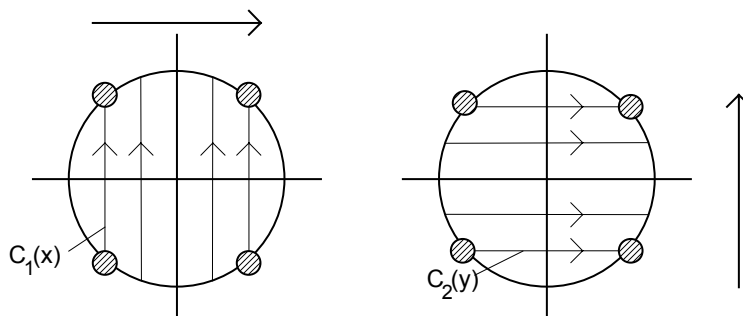


Figure 4.3. Locations of $C_1(x)$ and $C_2(y)$.

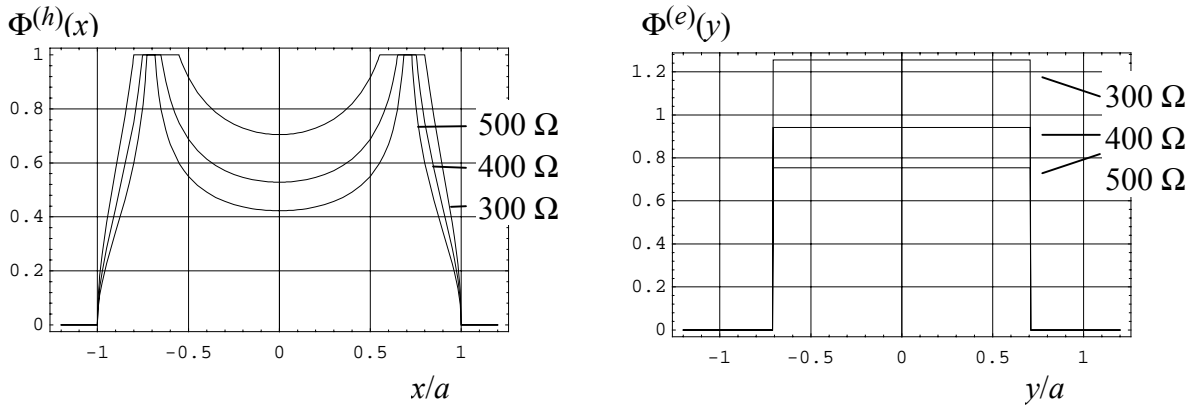


Figure 4.4. The normalized potential functions, $\Phi^{(h)}(x)$ and $\Phi^{(e)}(y)$, for a few different impedances.

The normalized potential for the E-plane is expressed as

$$\Phi^{(e)}(y) = -\frac{1}{(2V_o)} \int_{C_2(y)} E_y dx = \frac{1}{\Delta u} \int_{C_2(y)} \frac{\partial u}{\partial y} dx \quad (4.7)$$

where $C_2(y)$ is a horizontal linear cut through the aperture plane, as shown in Figure 4.3. To evaluate this, we require the Cauchy-Riemann relation for analytic functions,

$$\frac{\partial u}{\partial y} = -\frac{\partial v}{\partial x} \quad (4.8)$$

which allows us to recast the integral as

$$\Phi^{(e)}(y) = \frac{-2}{\Delta u} \left[v\left(\sqrt{a^2 - y^2}, y\right) - v(0, y) \right] \quad (4.9)$$

This is a particularly simple form, because the edges of the circular aperture are also lines of constant v . Thus, the normalized potential is evaluated analytically as

$$\Phi^{(e)}(y) = \begin{cases} 1/f_g & |y|/a < 1/\sqrt{2} \\ 0 & \text{else} \end{cases} \quad (4.10)$$

Note that we show a very abrupt transition between the two values, but it is actually more smooth. This transition occurs as $C_2(y)$ passes through the two wires, and if the wire is thin, an abrupt transition is an excellent approximation. We have plotted the normalized potentials for a few impedances in Figure 4.4 (right).

With the normalized potentials calculated, we can now calculate the radiated field as a function of angle off boresight in the H and E-planes. The H-plane and E-plane are the planes that are perpendicular and parallel to the dominant radiated field on boresight, respectively. In the H-plane and E-plane, the field radiated by a step voltage of magnitude $2V_o$ across the aperture is [13]

$$\begin{aligned} E_{step}^{(h)}(r, \theta, t) &= 1_y \left(\frac{-(2V_o)}{r} \right) \frac{\cot(\theta)}{2\pi} \Phi^{(h)}\left(\frac{ct}{a \sin(\theta)}\right) \\ E_{step}^{(e)}(r, \theta, t) &= \pm 1_\theta \left(\frac{-(2V_o)}{r} \right) \frac{1}{2\pi \sin(\theta)} \Phi^{(e)}\left(\frac{ct}{a \sin(\theta)}\right) \end{aligned} \quad (4.11)$$

In Figure 4.5 we have plotted these for the case of diameter = $2a = 22.9$ cm, for a four-arm feed with 200Ω input impedance. Time plots of these two step responses are shown for a few different values off-boresight in the H and E-planes. Note that we cannot plot the step response at 0° , because it is a delta function there, with infinite magnitude and zero width.

To obtain a radiated field, we convolve the step responses with the derivative of the driving voltage. To drive the antenna, we assume an integrated Gaussian with a peak magnitude of V_o and a risetime of $t_d = 50$ ps. We have plotted the time response at $\theta = 0^\circ, 2.5^\circ, 5^\circ, 10^\circ$ and 20° away from boresight in the E and H planes, in Figure 4.6.

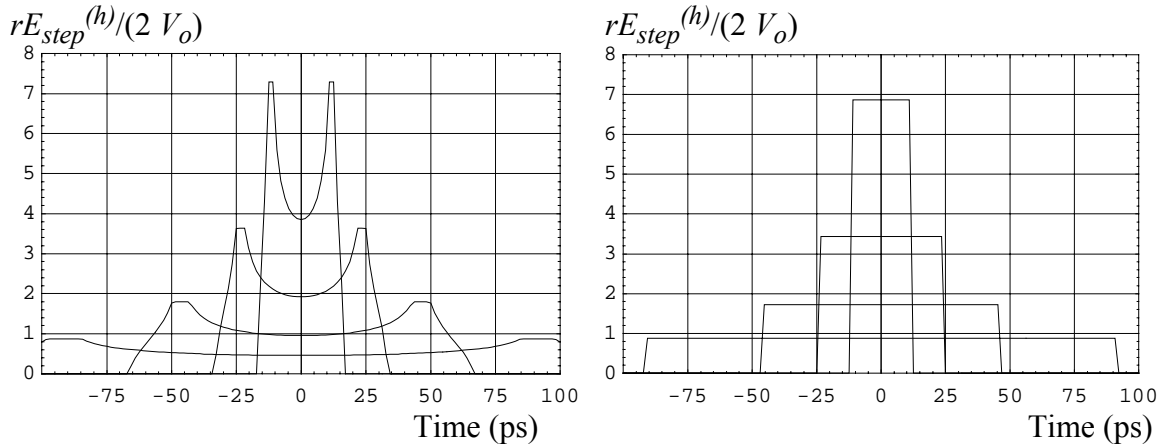


Figure 4.5. Step response of the 4-armed reflector IRA in the H-plane (left) and the E-plane (right), at $2.5^\circ, 5^\circ, 10^\circ$, and 20° degrees off-boresight.

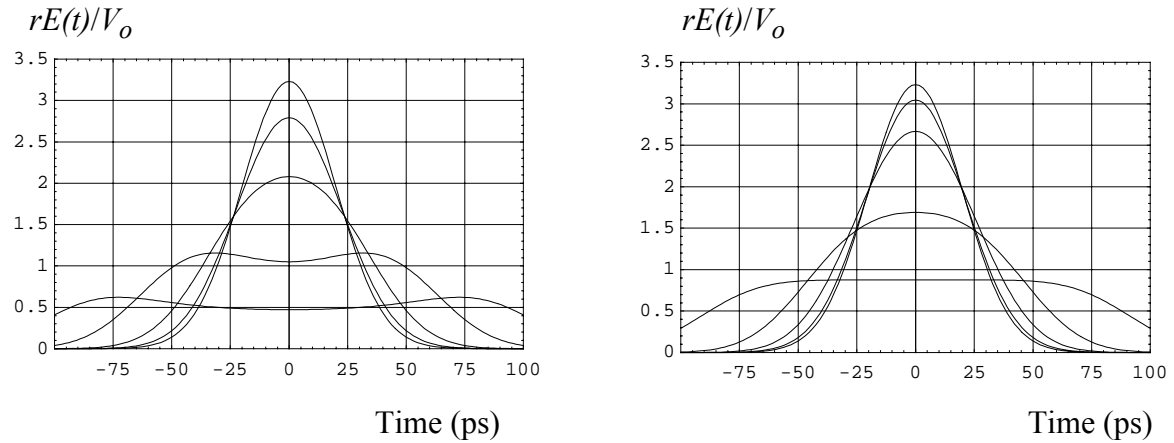


Figure 4.6. Fast part of the H-plane (left) and E-plane (right) radiated field for the reflector IRA at $\theta = 0^\circ, 2.5^\circ, 5^\circ, 10^\circ$ and 20° away from boresight.

VI. CONCLUSION

We have considered here a number of extensions to IRA theory, including an assortment of new IRA designs using two reflecting or refracting surfaces. We have also considered the optimal impedance for a long TEM horn or lens IRA, and we have calculated the off-boresight field radiated from a four-wire aperture.

ACKNOWLEDGMENTS

Dr. Charles A. Frost, of Pulse Power Physics, first suggested the Solid Dielectric Lens IRA. Dr. Gary D. Sower, of EG&G MSI, suggested an early version of the Split IRA.

REFERENCES

1. C. E. Baum and E. G. Farr, "Impulse Radiating Antennas," pp. 139-147 in H. L. Bertoni et al (eds.), *Ultra Wideband/Short-Pulse Electromagnetics*, Plenum Press, New York, 1993.
2. E. G. Farr, C. E. Baum, and C. J. Buchenauer, "Impulse Radiating Antennas, Part II," pp. 159-178 in L. Carin et al (eds.), *Ultra Wideband/Short-Pulse Electromagnetics 2*, Plenum Press, New York, 1995.
3. E. G. Farr and C. E. Baum, Impulse Radiating Antennas With Two Refracting or Reflecting Surfaces, Sensor and Simulation Note 379, May 1995.
4. C. E. Baum, J. J. Sadler, and A. P. Stone, Uniform Isotropic Dielectric Equal-Time Lenses for Matching Combinations of Plane and Spherical Waves, Sensor and Simulation Note 352, December 1992.
5. E. G. Farr, Optimizing the Feed Impedance of Impulse Radiating Antennas, Part I: Reflector IRAs, Sensor and Simulation Note 354, January 1993.
6. E. G. Farr, Optimization of the Feed Impedance of Impulse Radiating Antennas, Part II: TEM Horns and Lens IRAs, Sensor and Simulation Note 384, November 1995.
7. C. E. Baum, D. V. Giri, and R. D. Gonzalez, Electromagnetic Field Distribution of the TEM Mode in a Symmetrical Two-Parallel-Plate Transmission Line, Sensor and Simulation Note 219, April 1976.
8. C. E. Baum, Impedances and Field Distributions for Parallel Plate Transmission Line Simulators, Sensor and Simulation Note 21, June 1966.
9. P. Moon and D. E. Spencer, *Field Theory Handbook*, second edition, Springer-Verlag, Berlin, 1971.
10. E. G. Farr and C. E. Baum, Extending the Definitions of Antenna Gain and Radiation Pattern Into the Time Domain, Sensor and Simulation Note 350, November 1992.
11. C. E. Baum, Aperture Efficiencies for IRAs, Sensor and Simulation Note 328, June 1991.
12. E. G. Farr and C. E. Baum, Radiation from Self-Reciprocal Apertures, Chapter 6 in C. E. Baum and H. N. Kritikos, *Electromagnetic Symmetry*, Taylor and Francis, 1995.
13. E. G. Farr and C. E. Baum, The Radiation Pattern of Reflector Impulse Radiating Antennas: Early-Time Response, Sensor and Simulation Note 358, June, 1993.
14. E. G. Farr and C. A. Frost, Development of a Reflector IRA and a Solid Dielectric Lens IRA, Part I: Design, Predictions and Construction, Sensor and Simulation Note 396, April 1996.